Eur. Phys. J. D **38**, 507–514 (2006)
DOI: 10.1140/epjd/e2006-00038-x

THE EUROPEAN PHYSICAL JOURNAL D

Electron correlations in a C_{20} fullerene cluster

A lattice density-functional study of the Hubbard model

R. López-Sandoval[1,2] and G.M. Pastor[2,3,a]

[1] Instituto Potosino de Investigación Científica y Tecnológica, Camino a la presa San José 2055, 78216 San Luis Potosí, México
[2] Laboratoire de Physique Quantique, Centre National de la Recherche Scientifique, Université Paul Sabatier, 118 route de Narbonne, 31062 Toulouse, France
[3] Laboratoire de Nanophysique Magnétisme et Optoélectronique, Institut National des Sciences Appliquées, 135 avenue de Rangueil, 31062 Toulouse, France

Received 15 June 2005 / Received in final form 27 September 2005
Published online 21 February 2006 –

Abstract. The ground-state properties of C_{20} fullerene clusters are determined in the framework of the Hubbard model by using lattice density-functional theory (LDFT) and scaling approximations to the interaction-energy functional. Results are given for the ground-state energy, kinetic and Coulomb energies, local magnetic moments, and charge-excitation gap, as a function of the Coulomb repulsion U/t and for electron or hole doping δ close to half-band filling ($|\delta| \leq 1$). The role of electron correlations is analyzed by comparing the LDFT results with fully unrestricted Hartree-Fock (UHF) calculations which take into account possible noncollinear arrangements of the local spin-polarizations. The consequences of the spin-density-wave symmetry breaking, often found in UHF, and the implications of this study for more complex fullerene structures are discussed.

PACS. 36.40.Cg Electronic and magnetic properties of clusters – 71.10.Fd Lattice fermion models (Hubbard model, etc.) – 73.22.-f Electronic structure of nanoscale materials: clusters, nanoparticles, nanotubes, and nanocrystals

1 Introduction

The discovery of the C_{60} fullerene [1] and the remarkable physical and chemical properties resulting from its unique topology and electronic structure have motivated an extraordinary research activity in past years [2]. One of the recent questions of interest in this field is the possibility of producing even smaller C or Si cagelike clusters and to synthesize novel solids using them as building blocks. Thus, several experimental and theoretical studies have been performed in order to elucidate the complex mechanisms of formation of these nanostructures [3–9]. In the particular case of C_{20}, which is expected to be the smallest fullerene, experiments indicate that the dominant species in laser-vaporization of graphite are ring structures, while theory yields different isomers depending on the calculation method [10–17]. Hartree-Fock (HF) studies predict that the ring is the lowest-energy isomer, followed by the bowl (a substructure of the C_{60} fullerene) and then by the dodecahedral cage [14–16]. In contrast, the local density approximation (LDA) to density-functional theory (DFT) yields the cage to be more stable than the bowl and the ring, whereas in a generalized gradient approximation (GGA) the same ordering as HF is obtained [14–16]. These investigations, as well as quantum Monte Carlo (QMC) calculations [17], indicate that non-trivial electron correlation effects play a central role in the structural and electronic properties of these nanoclusters.

Recently, Prinzbach and coworkers succeeded to produce the cage-structured fullerene C_{20} in the gas phase starting from the perhydrogenated form $C_{20}H_{20}$ [6]. This isomer, which is not formed spontaneously in carbon condensation or cluster annealing processes, has a sufficiently long lifetime. Moreover, photoelectron spectrum (PES) measurements have been performed from which its cage-like structure has been inferred [6]. Theoretical studies by Saito and Miyamoto have reproduced the PES thereby confirming the structure assignment given in experiment [7]. In addition, experimental evidence has been provided on the oligomerization of C_{20} fullerenes [8] and on the formation of a solid phase of C_{20} dodecahedra [9] which, unlike C_{60} solids, involve strong C–C bonds between the pentagons of neighboring units.

Besides its experimental realization, the topology of C_{20} appears to be a particularly attractive physical

[a] e-mail: gustavo.pastor@irsamc.ups-tlse.fr

situation for theoretical investigations of correlated itinerant electrons in cagelike clusters with pentagonal rings. Similar studies on C_{12} and C_{60} clusters have already been performed in relation to alkali-metal-doped C_{60} solids like K_3C_{60} and Rb_3C_{60} [18], since one expects that the basic physics behind the superconducting and optical properties of these materials should be captured at the scale of an individual molecular constituent. The smaller fullerenes have attracted a special attention in this context due to the perspective of achieving larger superconducting transition temperatures than the C_{60}-based solids. Indeed, a number of theoretical investigations predict a significant enhancement of the electron-phonon coupling as the size of the fullerene is reduced from C_{60} to C_{36}, C_{28}, and finally C_{20} [5,19,20]. Consequently, theoretical studies aiming at understanding the properties of correlated electrons in small fullerene clusters are of considerable interest.

Lattice models have been used to determine low-energy properties of C_{60} which derive from the outermost half-filled π-electron cloud. In particular, the spin-density distribution on the buckyball has been analyzed in a series of papers [21–26]. Coffey and Trugman [21] calculated the ground-state spin configuration using a classical antiferromagnetic (AF) Heisenberg Hamiltonian corresponding to the strongly correlated limit of the Hubbard model. They found that the lowest-energy spin structure shows a nontrivial noncollinear order which minimizes magnetic frustrations within each pentagonal ring, keeping strong AF short-range order in bonds connecting nearest neighbor (NN) pentagons [21]. The spin structure in C_{60} was also investigated by means of Hubbard or Pariser-Parr-Pople Hamiltonians at half-band filling, taking into account on-site and inter-site Coulomb interactions within the unrestricted Hartree-Fock (UHF) approximation [23–26]. A common result of these investigations is the presence of a magnetic instability for a critical value U_c of the on-site Coulomb repulsion yielding a magnetic order which resembles that of the classical AF Heisenberg model. In addition remarkable noncollinear spin arrangements and charge-density redistributions have been obtained in mean-field calculations as a function of electron and hole doping [26]. QMC simulations on C_{60} at half-band filling and exact diagonalization studies of cagelike C_{12} support the existence of non-vanishing short-range spin correlations [22,27]. However, it should be recalled that there is no experimental evidence for an spontaneous symmetry breaking. Instead, the spin-density-wave instability should be interpreted as an indication of fluctuating spin-spin correlations within the cluster. It is therefore interesting to improve on the treatment of correlations in order to quantify the possible effects of artificial symmetry breaking on the electronic properties.

The purpose of this paper is to investigate the ground-state properties of correlated electrons on a C_{20} cagelike cluster by using the Hubbard Hamiltonian and a recently developed lattice density-functional theory (LDFT) [28,29]. Previous applications of this approach to 1D and 2D lattices have yield quite accurate ground-state properties for all band fillings and interaction regimes. A particularly interesting feature in the present context is that LDFT does not necessarily involve a symmetry breaking in order to account for the effects of electron correlation and localization in the strongly interacting limit [29]. Thus, it appears as an appropriate means of improving on UHF calculations. Moreover, besides the aspects specifically related to C_{20} and its topology, the present calculations should be of interest as a finite cluster application of new density-functional approaches to lattice fermion models [30].

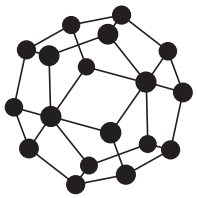

Fig. 1. Illustration of the geometry of the cagelike C_{20} cluster.

The body of the paper is organized as follows. In Section 2 the model Hamiltonian and the main steps in the formulation of LDFT are briefly recalled. Results for the ground-state energy, kinetic and Coulomb energies, local magnetic moments, and charge excitation gap of C_{20} are presented and discussed in Section 3 as a function of Coulomb repulsion U/t and for electron or hole dopings δ close to half-band filling ($|\delta| \leq 1$). Finally, Section 4 summarizes the main conclusions and discusses some perspectives of extensions in view of applications to lower symmetry structures.

2 Model Hamiltonian and calculation method

We consider the Hubbard Hamiltonian [31]

$$H = -t \sum_{\langle i,j\rangle\sigma} \hat{c}^{\dagger}_{i\sigma}\hat{c}_{j\sigma} + U \sum_{i} \hat{n}_{i\downarrow}\hat{n}_{i\uparrow}, \qquad (1)$$

on the C_{20} structure illustrated in Figure 1. In the usual notation, $\hat{c}^{\dagger}_{i\sigma}$ ($\hat{c}_{i\sigma}$) refers to the creation (annihilation) operator of an electron with spin σ at site i, and $\hat{n}_{i\sigma} = \hat{c}^{\dagger}_{i\sigma}\hat{c}_{i\sigma}$ to the corresponding number operator. The first term is the kinetic-energy operator with hopping integrals $t_{ij} = -t < 0$ for NNs and $t_{ij} = 0$ otherwise. The second term takes into account intraatomic interactions by means of the on-site Coulomb repulsion integral U. Given the lattice structure and the number of atoms $N_a = 20$, the model is characterized by the number of electrons N_e, or doping $\delta = N_e - N_a$, and by the ratio U/t.

In order to determine the ground-state properties we consider a density-functional approach to electron correlations in a lattice, in which the fundamental variable is the single-particle density matrix γ_{ij} [29]. The ground-state energy E_{gs} and density matrix γ^{gs}_{ij} are determined by minimizing the energy functional

$$E[\gamma] = E_K[\gamma] + W[\gamma] \qquad (2)$$

with respect to γ_{ij}. The first term in equation (2) is the kinetic energy

$$E_K[\gamma] = \sum_{ij} t_{ij}\gamma_{ij} \tag{3}$$

associated with the electronic motion in the lattice. The second term is the interaction-energy functional, formally given by [32]

$$W[\gamma] = \min_{\Psi\to\gamma}\left[U\sum_i \langle\Psi[\gamma]|\hat{n}_{i\uparrow}\hat{n}_{i\downarrow}|\Psi[\gamma]\rangle\right], \tag{4}$$

where the constrained minimization runs over all N-particle states $|\Psi[\gamma]\rangle$ that satisfy

$$\langle\Psi[\gamma]|\sum_\sigma \hat{c}^\dagger_{i\sigma}\hat{c}_{j\sigma}\,|\Psi[\gamma]\rangle = \gamma_{ij} \tag{5}$$

for all i and j. Thus, W represents the minimum value of the interaction energy compatible with a given degree of electron delocalization or density matrix γ_{ij}. The universal functional $W[\gamma]$, valid for all lattice structures and hybridizations, can be considerably simplified if the hopping integrals are short ranged. For example, if only NN hoppings are considered as in the present case, the kinetic energy E_K is independent of the density-matrix elements between sites that are not NNs. Therefore, the constrained search in equation (4) may be restricted to the $|\Psi[\gamma]\rangle$ that satisfy equation (5) only for $i = j$ and for NN ij. Moreover, for highly symmetric clusters like C_{20}, one has the same equilibrium value of γ_{ij} for all NN pairs ij, and $\gamma_{ii} = n = N_e/N_a$ for all sites i. The interaction energy can then be regarded as a simple function $W(\gamma_{ij})$ of the density-matrix element between NNs. However, notice that restricting the minimization constraints in equations (4) and (5) to NN γ_{ij} also implies that W loses its universal character, since the NN map and the resulting dependence of W on γ_{ij} are in principle different for different lattice structures [28,29].

Two previously investigated scaling approximations to the interaction energy W of the Hubbard model shall be used for the calculations [29,33]. In the first one the functional dependence is derived from the exact solution of equation (4) for the Hubbard dimer. It is given by [29]

$$W^{(2)} = E_{\rm HF}\left(1-\sqrt{1-g_{ij}^2}\right), \tag{6}$$

where $E_{\rm HF} = N_aUn^2/4$ refers to the Hartree-Fock energy and $g_{ij} = (\gamma_{ij}-\gamma_{ij}^\infty)/(\gamma_{ij}^0-\gamma_{ij}^\infty)$ measures the degree of electron correlation in a NN bond ij. Here, $\gamma_{ij}^0 > 0$ stands for the largest possible value of the bond order γ_{ij} for a given N_a, band filling $n = N_e/N_a$, and lattice structure. It represents the maximum degree of electron delocalization regardless of correlations. γ_{ij}^∞ refers to the strongly correlated limit of γ_{ij}, i.e., to the largest NN bond order that can be achieved under the constraint of vanishing W. For half-band filling $\gamma_{ij}^\infty = 0$, while for $n \neq 1$, $\gamma_{ij}^\infty > 0$ [34]. Thus, $g_{ij} = 1$ in an uncorrelated state, and $g_{ij} = 0$ in the strongly correlated limit corresponding, for example, to a fully localized or fully spin-polarized state (Nagaoka state). Physically, the scaling hypothesis underlying equation (6) means that the relative change in W associated with a given change in g_{12} is considered as independent of the system under study. Exact numerical studies of the functional dependence of W have shown that this is a good approximation in a wide variety of 1D, 2D, and 3D lattices and band fillings [28]. Notice that $E_{\rm HF}$, γ_{12}^∞, and γ_{12}^0 are system specific. In practice, γ_{12}^∞ is approximated by the ferromagnetic fully-polarized $\gamma_{12}^{\rm FM}$ which can be obtained, as $E_{\rm HF}$ and γ_{12}^0, from the single-particle electronic structure.

The dimer approximation to W is very appealing since it combines remarkable simplicity and good accuracy [29,35]. Nevertheless, it also presents some limitations particularly in the limit of strong correlations at half-band filling. For $N_e = N_a$ and small γ_{ij}, $W^{(2)}$ can be expanded as $W^{(2)} = (1/8)\alpha_2 U\gamma_{ij}^2 + \mathcal{O}(\gamma_{ij}^4)$ with $\alpha_2 = (\gamma_{ij}^0)^{-2}$ (e.g., $\alpha_2 = 2.92$ for a pentagonal ring and $\alpha_2 = 4.16$ for C_{20}). The exact functional W shows the same behavior but usually with a somewhat larger coefficient α_{ex} (e.g., $\alpha_{ex} = 3.21$ for a pentagonal ring and $\alpha_2 = 5.22$ for C_{20}) [36]. These discrepancies have direct consequences on the resulting ground-state properties for $U/t \gg 1$, since in this limit $\gamma_{ij}^{gs} \simeq (4z/\alpha)(t/U)$ and $E_{gs} \simeq -(2z^2/\alpha)(t^2/U)$, where z is the local coordination number ($E_K = -zt\gamma_{ij}$). In order to improve the accuracy a more flexible approximation has been proposed which is also based on the scaling properties of W, and which recovers the exact dependence on γ_{ij} for $\gamma_{ij} \to 0$. In this case the interaction energy includes a fourth-order term in g_{ij} and is given by

$$W^{(4)} = E_{\rm HF}\left(1-\sqrt{1-\kappa g_{ij}^2+(\kappa-1)g_{ij}^4}\right), \tag{7}$$

where $\kappa = \alpha_{ex}/\alpha_2$. In a pentagonal ring $\kappa = 1.10$, while in the C_{20} cluster $\kappa = 1.26$. These values should be compared with the dimer result $\kappa = 1$, for which equation (7) reduces to equation (6). Thus, the 4th-order term appears as a moderate correction to the dimer or 2nd-order approximation ($g_{ij}^2 \leq 1$). Previous applications to 1D and 2D systems have shown that equation (7) provides a systematic improvement on the ground-state properties for all U/t [33]. In the following section, equations (6) and (7) are applied to determine several electronic properties of the C_{20} Hubbard cluster in the framework of LDFT.

3 Results

The Hubbard model is characterized by the dimensionless parameter U/t and by the number of electrons N_e or the doping $\delta = N_e - N_a$. We consider the complete range of repulsive interactions ($U \geq 0$) and single electron or hole dopings ($|\delta| \leq 1$). The value of U/t gives a measure of the importance of correlation effects. Realistic estimates of U and t for C_{60} are $U \simeq 9$ eV and $t \simeq 2$–3 eV [38, 39]. Thus, commonly accepted values of U/t for the π-electrons in carbon fullerenes fall into the intermediate range $2 \leq U/t \leq 5$ [23–26]. As it will be discussed

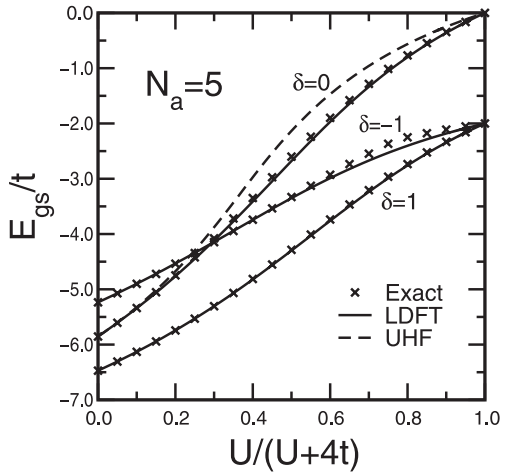

Fig. 2. Ground-state energy E_{gs} of the Hubbard model on a pentagonal ring as a function of Coulomb interaction U/t for different numbers of electrons $N_e = N_a + \delta$ close to half-band filling ($N_a = 5$) [40]. For $\delta = 1$, results for $E_{gs} - U$ are shown. The solid curves correspond to lattice density-functional theory (LDFT), the crosses to exact numerical diagonalizations, and the dashed curve for $\delta = 0$ to unrestricted Hartree-Fock (UHF) calculations including noncollinear spin arrangements.

below, this corresponds to a crossover between weakly-interacting delocalized electrons and strongly-correlated localized states. It is therefore, interesting to investigate the electronic properties in the full interaction range, particularly in order to follow the changes from weak to strong interactions, and to approach the crossover behavior from both sides.

Before discussing the results for the C_{20} cluster it is useful to consider a single pentagonal ring as a preliminary test on the accuracy of the method, since the pentagon constitutes the basic building block of the C_{20} structure, and since it is small enough so that exact diagonalizations can be easily performed. Figure 2 shows results for the ground-state energy E_{gs} of the $N_a = 5$ ring as a function of U/t [40]. In the uncorrelated limit E_{gs} decreases monotonously with increasing number of electrons $N_e = N_a + \delta \leq 6$ since the three lowest single-particle eigenvalues of the ring are negative. On the other side, for large U/t, E_{gs} vanishes at half-band filling while for negative (positive) doping E_{gs} ($E_{gs} - U\delta$) remains negative. In fact, for $\delta = 0$ the suppression of charge fluctuations always implies electron localization, whereas for $|\delta| = 1$ a finite kinetic energy persists, even for $U/t \gg 1$, due to the delocalization of the extra electron or hole. The LDFT calculations reproduce remarkably well the crossover between weak and strong correlations as given by the exact diagonalizations. Appreciable discrepancies are found only for $\delta = -1$ and $U/t \geq 6$, in which case the largest relative error amounts to $|E_{gs}^{LDFT} - E_{gs}^{ex}|/|E_{gs}^{ex}| \simeq 0.07$ for $U/t \simeq 12$. In the other cases ($\delta = 0$ or 1) the LDFT results are practically indistinguishable from the exact ones.

In order to quantify the effects of electron correlations we have also performed calculations by using the fully unrestricted Hartree-Fock (UHF) approximation which corresponds to the most general single-Slater-determinant wave-function and which allows for noncollinear site-dependent spin polarizations $\langle \vec{S}_i \rangle$ [26]. Figure 2 shows the UHF results for E_{gs} of the pentagonal ring at half-band filling ($\delta = 0$). For $U/t < U_c \simeq 0.27$ the only solution to the self-consistent equations is non-magnetic (i.e., $\langle \vec{S}_i \rangle = 0$ for all i), while for $U/t > U_c$ local magnetic moments $\langle \vec{S}_i \rangle$ set in. These increase monotonously with U/t reaching saturation in the limit of $U/t \to \infty$. Concerning the magnetic order one observes that the $\langle \vec{S}_i \rangle$ are all coplanar and that the angle between NN moments is $4\pi/5$ for all $U/t > U_c$. This amounts to split one parallel-spin frustration among five bonds which corresponds, as expected for half-band filling, to the solution of a classical Heisenberg model with antiferromagnetic NN interactions. One observes that UHF reproduces the U/t dependence of E_{gs} qualitatively well, including the strongly correlated limit where $E_{gs} \to 0$. This is achieved by localizing the electrons through the formation of increasingly large local magnetic moments as U/t increases. Nevertheless, significant quantitative discrepancies with the exact numerical solution are observed already for $U/t \geq 2$, which reflect the importance of electron-correlation effects. These can be regarded in part as the result of fluctuations between different spin configurations which cannot be recovered in a single-determinant state [42]. In contrast, LDFT gives a much better description of the ground-state, particularly in the intermediate and strong interacting regimes. UHF overestimates E_{gs} appreciably, while the differences between exact and LDFT results are very small.

More detailed information on the correlation effects and on the accuracy of the calculations is obtained from the kinetic energy E_K, Coulomb energy E_C, and local square magnetic moments $\langle S_i^2 \rangle$ presented in Figure 3. LDFT accurately reproduces the exact numerical solution, showing that the very good results obtained for E_{gs} are not the consequence of important compensations of errors. Moreover, the differences between 2nd-order and 4th-order approximations to W [see Eqs. (6) and (7)] are quite small, typically of the order of the differences between the 4th-order calculations and the exact results. Nevertheless, one may observe that the interaction-energy functional $W^{(4)}$ provides a consistent improvement with respect to $W^{(2)}$. In fact taking into account the 4th-order term yields a small increase (reduction) of E_C for $U/t < 4$ ($U/t > 4$) as well as a small reduction of $|E_K|$ for $U/t > 4$ which bring the outcome of LDFT systematically closer to the exact solution [41].

In contrast to LDFT the UHF calculations do not provide a correct description of the kinetic and Coulomb energies separately. On the one side, for $U/t < 4$, UHF overestimates the Coulomb energy E_C due to an underestimation of the local moments $\langle S_i^2 \rangle$ (see Fig. 3). On the other side, for $U/t > 4$, both E_C and $|E_K|$ are appreciably underestimated. The inaccuracies in E_C and $|E_K|$ for $U/t > 4$ tend to cancel each other, which improves to some extent the UHF result for E_{gs} (see Fig. 2). Notice that UHF reproduces quite accurately the local moments for $U/t > 4$ (see Fig. 3). However, a single-determinant state

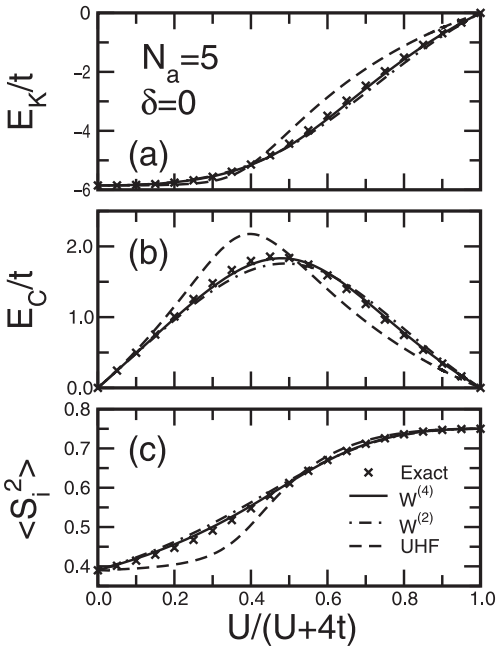

Fig. 3. (a) Kinetic energy E_K, (b) Coulomb energy E_C, and (c) local magnetic moments $\langle S_i^2 \rangle$ of the Hubbard model on a pentagonal ring at half-band filling ($N_e = N_a = 5$). The dashed-dotted and full curves correspond to lattice density-functional theory (LDFT) using, respectively, equations (6) and (7) for the interaction-energy functional. The dashed curves refer to the unrestricted Hartree-Fock (UHF) calculations including noncollinear spin arrangements, and the crosses to exact numerical diagonalizations.

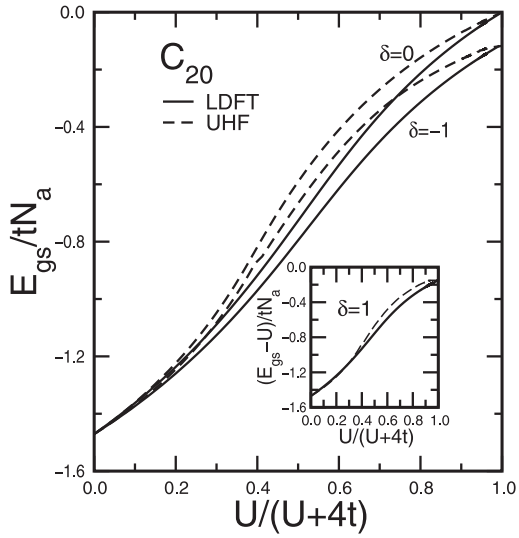

Fig. 4. Ground-state energy E_{gs} of the Hubbard model on the cagelike C_{20} cluster illustrated in Figure 1. Results are given as a function of Coulomb interaction U/t for different numbers of electrons $N_e = N_a + \delta$ close to half-band filling ($N_a = 20$) [40]. In the inset $E_{gs} - U$ is shown for $\delta = 1$. The solid curves correspond to lattice density-functional theory (LDFT) using equation (7) for the interaction-energy functional. The dashed curves refer to unrestricted Hartree-Fock (UHF) calculations including noncollinear spin arrangements.

fails to incorporate correlations, and in particular the fluctuations between different equivalent spin configurations, which should restore the broken spin symmetry and which are often important in finite systems [42]. This reflects the limitations of the broken symmetry UHF solutions, even in the most general noncollinear case [26]. Notice that in LDFT no artificial symmetry breaking is required in order to account for correlation-induced localizations and the resulting effects on the ground-state properties. The present LDFT formalism with the dimer or 4th-order scaling approximations to the interaction-energy functional describes correctly the electronic correlations in a pentagonal Hubbard ring. It can be therefore expected that the method should remain accurate in more complex systems with five-fold symmetry such as the C_{20} cluster to be discussed below. Moreover, comparison with exact results also shows that the differences between UHF and LDFT results for E_{gs}, E_K, and E_C are a good quantitative estimation of the correlation energies

In Figures 4 and 5 LDFT and UHF results are given for several ground-state properties of the Hubbard model on the cagelike C_{20} cluster illustrated in Figure 1. In the uncorrelated limit the ground-state energies E_{gs} are the same for $|\delta| \leq 1$, a consequence of the degeneracy of the single-particle spectrum. As U/t increases, E_{gs} increases monotonously with a slope $\partial E_{gs}/\partial U = \sum_i \langle n_{i\uparrow} n_{i\downarrow} \rangle > 0$. Since the average number of double occupations is larger

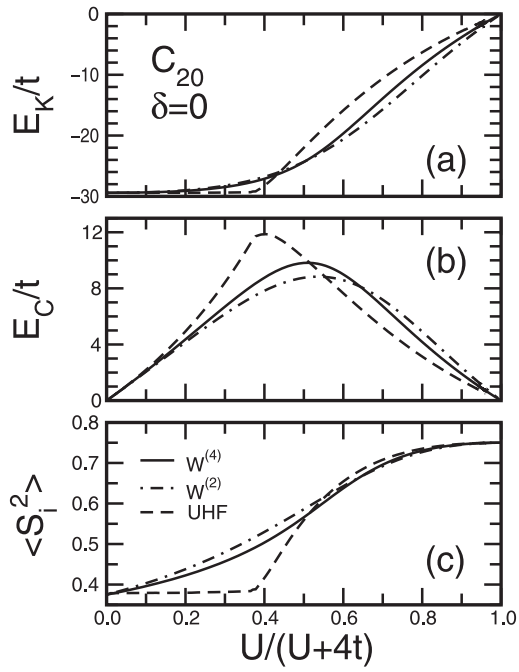

Fig. 5. (a) Kinetic energy E_K, (b) Coulomb energy E_C, and (c) local magnetic moments $\langle S_i^2 \rangle$ of the cagelike C_{20} Hubbard cluster at half-band filling ($\delta = 0$). The dashed-dotted and full curves correspond to lattice density-functional theory (LDFT) using, respectively, equations (6) and (7) for the interaction-energy functional. The dashed curves refer to unrestricted Hartree-Fock (UHF) calculations including noncollinear spin arrangements.

for larger number of electrons the degeneracy with respect to δ is removed at finite U/t. On the other side, in the strongly correlated limit, E_{gs} vanishes at half-band filling, while for $\delta = -1$ ($\delta = 1$) E_{gs} ($E_{gs} - U$) remains negative. The U/t dependence of E_{gs} in C_{20} follows similar trends as in the pentagonal ring [40]. The UHF calculations reproduce the exact limits for $U/t = 0$ and $U/t = \infty$, and agree qualitatively with LDFT for finite values of the Coulomb repulsion. However, the quantitative differences can be quite significant particularly for intermediate and large U/t (e.g., 26% for $U/t \simeq 36$). It is interesting to observe that electron correlations have also been found to play a central role in ab initio calculations of the ground-state energy of C_{10} and C_{20} isomers [17]. While the Hubbard Hamiltonian is probably too simple to determine accurately the binding energies of the various structures, it has been shown to provide an appropriate framework for assessing the importance of correlation effects in nanoclusters [43].

The effects of correlations are more significant in the kinetic energy E_K, Coulomb energy E_C, and local square moment $\langle S_i^2 \rangle$ shown in Figure 5 for $\delta = 0$. The differences between UHF and LDFT calculations for E_K and E_C are similar to the corresponding differences between UHF and exact results for the pentagonal ring and can be qualitatively understood in similar terms. In the case of C_{20} one may notice that the UHF results for the local square moment $\langle S_i^2 \rangle$ are the same as in the uncorrelated limit for $U/t < 2.2$. Therefore, they are significantly underestimated. For stronger Coulomb repulsions ($U/t > 2.2$) $\langle S_i^2 \rangle$ increases rapidly reaching values that are very close to the LDFT results for $U/t \simeq 4$ (see Fig. 5). This behavior is related to the U/t dependence of the self-consistent solution of the UHF equations. For $0 \leq U/t \leq 3.1$ the UHF charge distribution is not uniform due to the four-fold degeneracy of the single-particle spectrum at the Fermi energy. Moreover, for $U/t < 2.2$ the UHF ground state shows a weakly ferromagnetic solution with very small local spin polarizations. In this way advantage is taken from the single-particle degeneracy in order to reduce the Coulomb-repulsion energy without increasing significantly the kinetic energy. For $U/t > 2.2$ the system starts to develop an AF spin-density wave which coexists with a weak charge-density wave for $2.2 < U/t < 3.1$. Only for $U/t > 3.1$ the AF-like magnetic order valid for strong interactions is definitely settled and the charge distribution becomes then uniform throughout the cluster. An illustration of the UHF magnetic order in the large U/t regime is shown in Figure 6. Notice the noncollinearity of the local spin polarizations $\langle \vec{S}_i \rangle$, which form angles of about 138 degrees between NNs. This value is smaller than the angle between NN $\langle \vec{S}_i \rangle$ in an isolated pentagonal ring (144 degrees) because of frustration effects between the pentagons in the C_{20} topology (see Figs. 1 and 6). Further increase of the Coulomb repulsion beyond $U/t = 3.1$ only results in an increase of the size of the local moments keeping the magnetic order unchanged.

The charge excitation gap is given by

$$\Delta E_c = E_{gs}(N_e + 1) + E_{gs}(N_e - 1) - 2E_{gs}(N_e) \,, \quad (8)$$

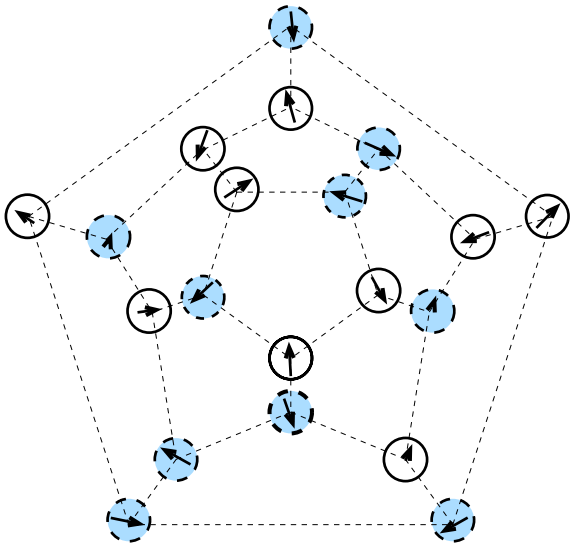

Fig. 6. Illustration of the distribution of the local spin polarizations $\langle \vec{S}_i \rangle$ in an undoped cagelike C_{20} cluster as obtained by using the Hubbard model and the unrestricted Hartree-Fock approximation ($\delta = 0$). Due to spin-rotational invariance only the relative orientations of $\langle \vec{S}_i \rangle$ are physically meaningful. The three-dimensional cluster structure (see Fig. 1) is mapped onto a plane in order to ease the visualization. The radius of the circle on each atomic site i is proportional to $|\langle \vec{S}_i \rangle|$. The arrows represent the projection of $\langle \vec{S}_i \rangle$ onto the xy-plane which is the plane containing the outermost pentagon. Shaded circles (open circles) indicate that the perpendicular component $\langle S_i^z \rangle$ is positive (negative).

where E_{gs} refers to ground-state energy. It is a property of considerable interest since it measures the low-energy excitations associated with changes in the number of electron N_e and is thus very sensitive to electron correlation effects. In Figure 7 results are shown for ΔE_c of the C_{20} Hubbard cluster at half-band filling ($N_e = N_a$). The corresponding calculations for the pentagonal ring are reported in the inset for the sake of comparison. At half-band filling $\Delta E_c = 0$ for $U = 0$, despite the finite size, due to the degeneracy of the single-particle spectrum in both the ring and C_{20}. ΔE_c increases with increasing U/t approaching the limit $\Delta E \to (U - w_b)$ for $U/t \to \infty$, where w_b is the bottom of single-particle spectrum of the cluster ($w_b = 2t$ for the ring and $w_b = 3t$ for C_{20}). The LDFT results and the exact calculations for $N_a = 5$ yield a linear dependence of ΔE_c as a function U/t for $U/t \ll 1$. This implies, in particular for C_{20}, that $\Delta E_c > 0$ for arbitrary small U/t, in contrast to the UHF result. Comparison with exact diagonalizations for $N_a = 5$ indicates that the LDFT gap is not overestimated. The UHF calculations fail to reproduce the correct U/t dependence of ΔE_c showing once more the importance of correlations. Notice that the differences between UHF and exact or LDFT results are qualitatively similar for C_{20} and for the pentagonal ring, which indicates that the contribution of correlations to ΔE_c are comparable in both cases.

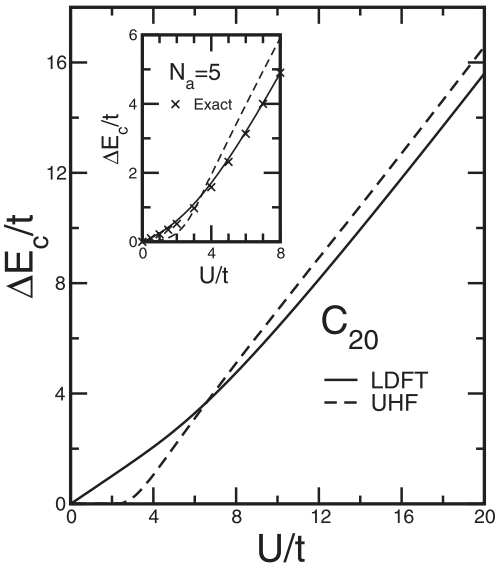

Fig. 7. Charge excitation gap ΔE_c of the Hubbard model on the cagelike C_{20} cluster as a function of Coulomb interaction U/t. The solid (dashed) curves correspond to LDFT (UHF). In the inset figure results are given for the pentagonal Hubbard ring. Here the crosses refer to exact diagonalizations.

4 Conclusion

A density-functional approach to lattice-fermion models has been applied to study the ground-state properties of the Hubbard Hamiltonian on a cagelike C_{20} cluster. The ground-state energy, the kinetic and Coulomb contributions, and the charge excitation gap have been determined as a function of U/t for dopings δ close to half band filling. The importance of electron correlations has been quantified by performing noncollinear Hartree-Fock calculations. Comparisons with exact diagonalizations and with UHF in the case of a pentagonal ring demonstrate the ability of LDFT to describe subtle correlation effects in a very simple and systematic way. It is therefore expected that LDFT should be an efficient tool for investigating the properties of strongly correlated fermions in more complex clusters and nanostructures, which are otherwise very difficult to tackle with other accurate methods.

The present LDFT study of clusters encourages the development of more flexible interaction-energy functionals in order to determine the properties of finite systems with lower symmetry. As a first step it would be interesting to extend the calculations to fullerene structures having different types of bonds, for example C_{60}. In these cases the functional dependence of $W[\gamma_{ij}]$ is more complex and one has to consider at least two different NN density-matrix elements, within and between pentagons, even if one assumes that the hopping integrals are the same. The symmetry of these bonds is actually different despite the fact that all sites are equivalent. The interaction-energy functional should be generalized following previous works on dimerized 1D chains [35]. The domain of representability of γ_{ij} and the accuracy of the scaling hypothesis could be explicitly tested for smaller similar clusters like C_{12} by solving Levy's constrained search [28,32]. Furthermore, the functional dependence of W for low-symmetry clusters deserves to be explored by taking into account charge transfers and eventual redistributions of the spin density between non-equivalent sites. This should open the way to investigations of correlation effects in a variety of complex physical situations such as metal clusters, disordered systems, and low-dimensional nanostructures.

This work has been supported by CONACyT Mexico (Grant No. J-41452 and Millennium Initiative W-8001) and by the EU GROWTH project AMMARE (Contract No. G5RD-CT-2001-00478). Computer resources were provided by IDRIS (CNRS, France).

References

1. H.W. Kroto, J.R. Heath, S.C. O'Brien, R.F. Curl, R.E. Smalley, Nature **318**, 162 (1985); W. Krätschmer, L.D. Lamb, K. Fostiropoulos, D.R. Huffman, Nature **347**, 354 (1990)
2. Y.H. Kim, I.H. Lee, K.J. Chang, S. Lee, Phys. Rev. Lett. **90**, 065501 (2003); Y. Zhao, B.Y. Yakobson, R.E. Smalley, Phys. Rev. Lett. **88**, 185501 (2002); D. Herschbach, Rev. Mod. Phys. **71**, S411 (1999); R.E. Smalley, Rev. Mod. Phys. **69**, 723 (1997)
3. U. Röthlisberger, W. Andreoni, M. Parrinello, Phys. Rev. Lett. **72**, 665 (1994); L. Mitas, J.C. Grossman, I. Stich, J. Tobik, Phys. Rev. Lett. **84**, 1479 (2000); Q. Sun, Q. Wang, P. Jena, B.K. Rao, Y. Kawazoe, Phys. Rev. Lett. **90**, 135503 (2003); D. Connétable et al., Phys. Rev. Lett. **91**, 247001 (2003); M.N. Huda, A.K. Ray, Eur. Phys. J. D **31**, 63 (2004)
4. C. Piskoti, J. Yarger, A. Zettl, Nature **393**, 771 (1998)
5. M. Coté, J.C. Grossman, M.L. Cohen, S.G. Louie, Phys. Rev. Lett. **81**, 697 (1998)
6. H. Prinzbach et al., Nature **407**, 60 (2000)
7. M. Saito, Y. Miyamoto, Phys. Rev. Lett. **87**, 035503 (2001)
8. R. Ehlich, P. Landenberger, H. Prinzbach, J. Chem. Phys. **155**, 5830 (2001)
9. Z. Iqbal et al., Eur. J. Phys. B **31**, 509 (2003)
10. G. von Helden, M.T. Hsu, N.G. Gotts, P.R. Kemper, M.T. Bowers, Chem. Phys. Lett. **204**, 15 (1993)
11. J.N. Hunter, J.L. Fey, M.F. Jarrold, J. Phys. Chem. **97**, 3460 (1993); J.N. Hunter, J.L. Fey, M.F. Jarrold, Science **260**, 784 (1993)
12. S. Yang, K.J. Taylor, M.J. Craycraft, J. Conceicao, C.L. Pettiete, O. Cheshnovsky, R.E. Smalley, Chem. Phys. Lett. **144**, 431 (1988)
13. H. Handschuh, G. Ganteför, B. Kessler, P.S. Bechthold, W. Eberhardt, Phys. Rev. Lett. **74**, 1095 (1995)
14. K. Raghavachari, D.L. Striut, G.K. Odom, G.E. Scuseria, J.A. Pople, B.G. Johnson, P.M.W. Gill, Chem. Phys. Lett. **214**, 357 (1993)
15. P.R. Taylor, E. Bylaska, J.H. Weare, R. Kawai, Chem. Phys. Lett. **235**, 538 (1995)
16. R.O. Jones, G. Seifert, Phys. Rev. Lett. **79**, 443 (1997); G. Galli, F. Gygi, J.-Christophe Golaz, Phys. Rev. B **57**, 1860 (1998)
17. J.C. Grossman, L. Mitas, K. Raghavachari, Phys. Rev. Lett. **75**, 3870 (1995)

18. A.F. Hebard et al., Nature **350**, 600 (1991); K. Holczer et al., Science **252**, 1154 (1991); Kroto et al., Nature **318**, 162 (1985)
19. N. Breda et al., Phys. Rev. B **62**, 130 (2000)
20. M. Saito, Y. Miyamoto, Phys. Rev. B **65**, 165434 (2002); J. Lu et al., Phys. Rev. B **67**, 125415 (2003)
21. D. Coffey, S.A. Trugman, Phys. Rev. Lett. **69**, 176 (1992)
22. D. Coffey, S.A. Trugman, Phys. Rev. B **46**, 12717 (1992)
23. L. Bergomi, J.P. Blaizot, Th. Jolicoeur, E. Dagotto, Phys. Rev. B **47**, R5539 (1993)
24. F. Willaime, L.M. Falicov, J. Chem. Phys. **98**, 6369 (1993)
25. P. Joyes, R.J. Tarento, Phys. Rev. B **45**, 12077 (1992); P. Joyes, R.J. Tarento, L. Bergomi, Phys. Rev. B **48**, 4855 (1993)
26. M.A. Ojeda, J. Dorantes-Dávila, G.M. Pastor, Phys. Rev. B **60**, 6121 (1999); M.A. Ojeda, J. Dorantes-Dávila, G.M. Pastor, Phys. Rev. B **60**, 9122 (1999)
27. R.T. Scalettar, A. Moreo, E. Dagotto, L. Bergomi, T. Jolicoeur, H. Monien, Phys. Rev. B **47**, 12316 (1993)
28. R. López-Sandoval, G.M. Pastor, Phys. Rev. B **61**, 1764 (2000)
29. R. López-Sandoval, G.M. Pastor, Phys. Rev. B **66**, 155118 (2002)
30. For alternative density-functional approaches to lattice-fermion models see, for instance, A.E. Carlsson, Phys. Rev. B **56**, 12058 (1997); R.G. Hennig, A.E. Carlsson, Phys. Rev. B **63**, 115116 (2001); N.A. Lima, M.F. Silva, L.N. Oliveira, K. Capelle, Phys. Rev. Lett. **90**, 146402 (2003)
31. J. Hubbard, Proc. R. Soc. Lond. A **276**, 238 (1963); J. Hubbard, Proc. R. Soc. Lond. A **281**, 401 (1964); J. Kanamori, Prog. Theo. Phys. **30**, 275 (1963); M.C. Gutzwiller, Phys. Rev. Lett. **10**, 159 (1963)
32. M. Levy, Proc. Natl. Acad. Sci. U.S.A. **76**, 6062 (1979)
33. R. López-Sandoval, G.M. Pastor, Phys. Rev. B **69**, 085101 (2004)
34. For simplicity, we focus here on $\gamma_{ij} > 0$ which is the relevant case for $t_{ij} = -t < 0$ [see Eq. (3)]. Consequently, we also consider only $\gamma_{ij}^{0} > 0$ and $\gamma_{ij}^{\infty} > 0$. However notice that in non-bipartite lattices as the C_{20} cluster the domains of representability for positive and negative values of the NN γ_{ij} are different. Therefore, one would have to distinguish the cases $0 \leq \gamma_{ij}^{\infty +} \leq \gamma_{ij} \leq \gamma_{ij}^{0+}$ from $\gamma_{ij}^{0-} \leq \gamma_{ij} \leq \gamma_{ij}^{\infty -} \leq 0$, since in non-bipartite lattices $\gamma_{ij}^{0-} \neq -\gamma_{ij}^{0+}$ and $\gamma_{ij}^{\infty -} \neq -\gamma_{ij}^{\infty +}$. Nevertheless, as shown in reference [28], the same scaling behavior of $W/E_{\rm HF}$ as a function of $g_{ij} = (\gamma_{ij} - \gamma_{ij}^{\infty -})/(\gamma_{ij}^{0-} - \gamma_{ij}^{\infty -})$ is found for $\gamma_{ij}^{0-} \leq \gamma_{ij} \leq \gamma_{ij}^{\infty -} \leq 0$. The situation is analogous to what is found in dimerized systems where the domain of representability $[\gamma^{\infty}(\phi), \gamma^{0}(\phi)]$ depends on the ratio $\gamma_{12}/\gamma_{23} = \tan\phi$ between the bond orders corresponding to short and long bonds (see Ref. [35]).
35. R. López-Sandoval, G.M. Pastor, Phys. Rev. B **67**, 035115 (2003)
36. The expansion coefficient of the exact functional W are here obtained from numerical exact diagonalizations for the Heisenberg limit of the Hubbard model ($\gamma_{ij} \to 0$). For extended systems or larger clusters they can be calculated by using degenerate perturbation theory (see Ref. [37])
37. M. Takahashi, J. Phys. C **10**, 1289 (1977)
38. S. Chakravarty, M.P. Gelfand, S. Kivelson, Science **254**, 970 (1991)
39. G. Stollhoff, Phys. Rev. B **44**, 10998 (1991)
40. The results are presented as a function of $\lambda = U/(U+4t)$ in order to cover the complete range of repulsive interactions $U/t \geq 0$ within a single plot ($0 \leq \lambda \leq 1$). In the weakly correlated limit ($U/t \ll 1$) $\lambda \simeq U/4t + O[(U/t)^2]$ and in the strongly correlated limit ($U/t \gg 1$) $\lambda \simeq 1 - 4t/U + O[(t/U)^2]$. Depending on the dimensions and structure of the system, the crossover between these two regimes is typically found for $\lambda \simeq 0.4$–0.7 where U/t is of the order of the single-particle band width.
41. A more detailed discussion of the accuracy of LDFT and the interaction-energy functionals may be found in references [29,33,35], where applications to periodic one-, two-, and three-dimensional systems are reported
42. L.M. Falicov, R.A. Harris, J. Chem. Phys. **51**, 3153 (1969); S.L. Reindl, G.M. Pastor, Phys. Rev. B **47**, 4680 (1993)
43. G.M. Pastor, R. Hirsch, B. Mühlschlegel, Phys. Rev. Lett. **72**, 3879 (1994); G.M. Pastor, R. Hirsch, B. Mühlschlegel, Phys. Rev. B **53**, 10382 (1996)